nanomaterials

MDPI

Article

Preparation and Characterization of Epoxy Resin Filled with $Ti_3C_2T_x$ MXene Nanosheets with Excellent Electric Conductivity

Ailing Feng [1], Tianqi Hou [2], Zirui Jia [2,*], Yi Zhang [2], Fan Zhang [3,*] and Guanglei Wu [2,4,*]

1 Institute of Physics & Optoelectronics Technology, Baoji University of Arts and Sciences, Baoji 721016, China; ailing@mail.xjtu.edu.cn
2 Institute of Materials for Energy and Environment, State Key Laboratory of Bio-Fibers and Eco-Textiles, College of Materials Science and Engineering, Qingdao University, Qingdao 266071, China; qdhoutq@163.com (T.H.); zhangy@njtech.edu.cn (Y.Z.)
3 School of Materials Sciences and Engineering, East China Jiaotong University, Nanchang 330013, China
4 Key Laboratory of Engineering Dielectrics and Its Application, Ministry of Education, Harbin University of Science and Technology, Harbin 150080, China
* Correspondence: jiazirui@mail.nwpu.edu.cn (Z.J.); zhang_fan2003@126.com (F.Z.); wuguanglei@qdu.edu.cn or wuguanglei@mail.xjtu.edu.cn (G.W.); Tel./Fax: +86-532-85951496 (G.W.)

Received: 14 December 2019; Accepted: 14 January 2020; Published: 17 January 2020

Abstract: MXene represents new kinds of two-dimensional material transition metal carbides and/or carbonitrides, which have attracted much attention in various applications including electrochemical storage devices, catalysts, and polymer composite. Here, we report a facile method to synthesize $Ti_3C_2T_x$ MXene nanosheets and prepare a novel electrically conductive adhesive based on epoxy resin filled with $Ti_3C_2T_x$ MXene nanosheets by solution blending. The structure, morphology, and performance of Ti_3C_2Tx MXene nanosheets and epoxy/$Ti_3C_2T_x$ MXene nanosheets composite were investigated. The results show that $Ti_3C_2T_x$ MXene possesses nanosheet structure. $Ti_3C_2T_x$ MXene nanosheets were homogeneously dispersed in epoxy resin. Electrical conductivity and mechanical properties measurements reveal that the epoxy/$Ti_3C_2T_x$ MXene nanosheet composite exhibited both good electrical conductivity (4.52×10^{-4} S/m) and favorable mechanical properties (tensile strength of 66.2 MPa and impact strength of 24.2 kJ/m^2) when the content of $Ti_3C_2T_x$ MXene nanosheets is 1.2 wt %. Thus, $Ti_3C_2T_x$ MXene is a promising filler for electrically conductive adhesive with high electric conductivity and high mechanical performance.

Keywords: MXene; epoxy resin; electrical conductivity; mechanical properties

1. Introduction

With the progression of science and technology, electronic units are developing towards the direction of miniaturization, portability, and high integration [1–5]. Therefore, the electronic packaging industry demands interconnect bonding technology, which could offer excellent electrical conductivity, good flexibility, and satisfied mechanical strength [6–9]. Besides, it should be cost effective and environmentally benign. In this regard, electrical conductive adhesives (ECAs) are regarded as one of the most feasible alternative interconnection materials for future applications due to low processing temperature, fine pitch interconnect, and environmental friendliness [10–13].

ECAs consist of polymer (such as, acrylate resin, silicone, or epoxy resin) and electrical conductive fillers (such as, Ag, Au, Ni, or carbon materials). The polymer resin provides interconnect bonding properties while conductive fillers conduct electricity in ECAs. This polymer is widely used because of its low density, high specific strength, dimensional stability, and chemical resistance [14–18].

Many researches have studied epoxy-based ECAs [19]. The formation of effective conductive paths in the ECAs is the key to obtain high electrical conductivity. Several conductive fillers have been studied in ECAs; these include cobalt nanoparticles [20], zinc complexes [21,22], cadmium [23], metal oxide [24], and so on. However, there are some issues such as aggregation and poor interconnect between conductive fillers with polymer resin, which need to be solved.

MXenes is a new kind of transition metal carbide/nitride two-dimensional material with graphene-like structure. Their chemical formulas are $M_{n+1}X_n$, where M is an early transition metal, X is C and/or N, and n represents the number of X (1, 2, or 3). MXenes are promising conductive fillers due to intrinsic high conductivity and unique structure [25–27]. Carbon materials (graphene or carbon nanotube) have to be oxidized to introduce oxygen-containing functional groups, which prevent carbon materials aggregating in the polymer resin and assist binding between graphene/carbon nanotube and EP resin. However, the appearance of some functional groups decreases the electronic conductivity. MXene does not require any pretreatment to composite with other materials, as the surface atomic of MXenes is Ti, which can easily bind the O atomic of EP resin. Therefore, MXenes could well be dispersed in the polymer resin and provide high electric conductivity.

Herein, we report on the structure and performance of EP/MXene ECAs. Ti_3AlC_2 was used as the MAX precursor to prepare $Ti_3C_2T_x$ MXene nanosheets. The crystal structure and morphology of $Ti_3C_2T_x$ MXene nanosheets were characterized by scanning electron microscope (SEM), X-ray diffraction (XRD), and transmission electron microscopy (TEM). Different amounts of $Ti_3C_2T_x$ MXene nanosheets were introduced into ECAs to study the effect of $Ti_3C_2T_x$ MXene nanosheets on the electrical properties and mechanical performance of the EP/$Ti_3C_2T_x$ MXene nanosheet ECAs. The results show that the electrical property and mechanical performance of the EP/$Ti_3C_2T_x$ MXene nanosheets ECAs could be improved compared to pure EP resin. Our work may shed lights on the development of ECAs with high electric conductivity and high mechanical performance in the electronic industry.

2. Experimental

2.1. Material

Epoxy resin and hardener tetrahyelrophthalic anhydride were purchased from Sigma-Aldrich. The titanium carbide (TiC) powders were obtained from Alfa Aesar. Commercially available Ti_2AlC was obtained from Kanthal Co., Ltd., Stockholm, Sweden; 36% hydrochloric acid (HCl) and lithium fluoride (LiF, 98%) were bought from Sinopharm Chemical Reagent Co., Ltd., Shanghai, China.

2.2. Preparation of EP/$Ti_3C_2T_x$ MXene Nanosheets ECAs

The Ti_3AlC_2 was prepared by mixing Ti_2AlC and TiC powders in a 1:1 M ratio, followed by ball-milling at 300 rpm for 18 h. After being milled, the mixture was heated to 1350 °C at 5 °C/min in an Al_2O_3 tube furnace under Ar atmosphere. Then, the mixture was reacted at 1350 °C for 2.0 h before cooling again. The resulting product is Ti_3AlC_2.

First, 0.66 g LiF was added in 6 M HCI solution; 1.0 g Ti_3AlC_2 powders were immersed in 50 mL LiF/HCl solution. The mixture was stirred for 48 h at 40 °C. The resulting suspension was washed using distilled water five times and centrifuged to separate the powder from the supernatant. Then, the obtained powder was sonicated for 2.0 h and rinsed three times with deionized water. $Ti_3C_2T_x$ MXene nanosheets were collected and dried in vacuum at 80 °C for 24 h.

The resin mixture was uniformly mixed at the epoxy resin and curing agent (methyl tetrahyelrophthalic anhydride) mass ratio equal to 100:32. Then, different amounts of $Ti_3C_2T_x$ MXene nanosheets added into resin mixture. To achieve uniform dispersion of $Ti_3C_2T_x$ MXene nanosheets in the epoxy resin, the mixture was mixed with a Flacktek Speed mixer at a speed of 2000 rpm for 0.5 h. The curing process took place at 100 °C for 2 h, 120 °C for 2 h and 160 °C for 4 h. After cooling to room temperature, the resulting EP/$Ti_3C_2T_x$ MXene nanosheets composites were obtained. The schematic illustration of preparation of EP/$Ti_3C_2T_x$ MXene nanosheets composites is illustrated in Figure 1.

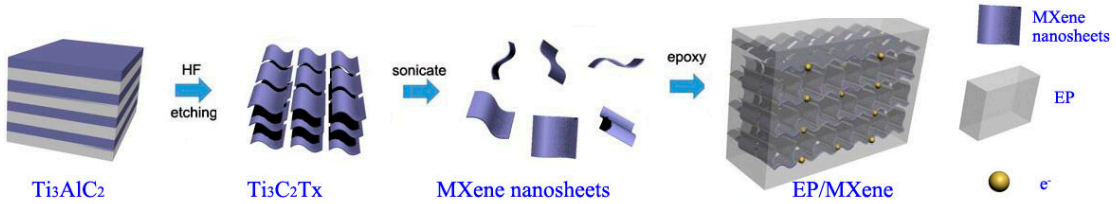

Figure 1. The schematic illustration for the synthetic procedure of the EP/$Ti_3C_2T_x$ MXene nanosheets composites.

2.3. Characterization and Measurement

The surface morphology of Ti_3AlC_2 and $Ti_3C_2T_x$ MXene nanosheets and the fracture surfaces of pure EP, EP/$Ti_3C_2T_x$ MXene nanosheets composites were characterized by SEM (FEI, Quanta 250, Washington, WA, USA). The element contents in $Ti_3C_2T_x$ MXene nanosheets were characterized by energy-dispersive X-ray (EDX, FEI, Quanta 250). The phase structures of Ti_3AlC_2 and $Ti_3C_2T_x$ MXene were characterized by X-ray powder diffraction (XRD, Rint-2000, Rigaku, Berlin, Germany) using Cu Kα radiation (λ = 1.5418 Å) operated at a voltage of 30 kV and a current of 10 mA. Fourier transform infrared spectrum (FTIR, IRpresitge-21 model, Tokyo, Japan) was used to record the Fourier transform infrared spectra of Ti_3AlC_2 and $Ti_3C_2T_x$ MXene. The internal morphology of $Ti_3C_2T_x$ MXene nanosheets were studied using transmission electron microscope (TEM, JEOL, JEM-2100 HT, Tokyo, Japan). There are four methods (Volt-Ampere, double bridge, direct current four probe, and digital multimeter) to measure the conductivity of composites. We used digital multimeter (830/F-33 model, Beijing Jiaxin Instrument, Ltd., Beijing, China) to test the resistance (R) of EP/$Ti_3C_2T_x$ MXene nanosheets composites. Composite circles with a diameter of 20 mm and a thickness of 2 mm were prepared. Then we calculated the resistivity (ρ) of composite based on the diameter and thickness of samples. Electrical conductivity (K) is the reciprocal of resistivity (ρ) as follows: $K = 0.0637/R$ (S/cm). The mechanical properties of EP/$Ti_3C_2T_x$ MXene nanosheets composites were tested using tensile testing machine (UTM-2460 model, Hebei JInjian Co., Ltd., Tangshan, China).

3. Results and Discussion

3.1. The Structure and Morphology of Ti_3AlC_2 and $Ti_3C_2T_x$ MXene

The SEM images of Ti_3AlC_2, $Ti_3C_2T_x$, and $Ti_3C_2T_x$ nanosheets are shown in Figure 2. SEM images (Figure 2a,b) show that Ti_3AlC_2 display a solid bulk morphology with uneven sizes. The smaller Ti_3AlC_2 MAX is about 2 μm while the larger one is about 20 μm. After HF etching, $Ti_3C_2T_x$ show a loosely packed structure consist of multilayered $Ti_3C_2T_x$ nanosheets, which had typical diameters of 2 μm (Figure 2c,d). The interlayer space of multilayered $Ti_3C_2T_x$ is ~200 nm. This morphology is because the LiF/HF treatment removes Al layers from Ti_3AlC_2 MAX. By sonication, the loosely packed $Ti_3C_2T_x$ MXene is converted to nanosheets (Figure 2e,f). The $Ti_3C_2T_x$ MXene nanosheets have smooth surface, which show a structure similar to that of graphene. The thin sheet is of ~10 nm thick, which corresponds to roughly 5 $Ti_3C_2T_x$ layers.

To study the elements of $Ti_3C_2T_x$ nanosheets, energy dispersive X-ray (EDX) analysis were carried out. Figure 3 reveal EDX spectrum and SEM-EDX element mappings of $Ti_3C_2T_x$ MXene nanosheets. As shown in Figure 3a, $Ti_3C_2T_x$ MXene thin nanosheets have diameters of 3 μm. In the EDX spectrum (Figure 3b), four strong peaks are belonged to C, Ti, O, and F, whereas a weak peak assigns to Al. As shown in Figure 3c, the uniform C, Ti, O, and F elemental distributions are observed. The composition of $Ti_3C_2T_x$ nanosheets, as calculated from EDS analysis, is shown in Table 1. The results showed that the $Ti_3C_2T_x$ MXene contains 11.0 wt % C, 69.0 wt % Ti, 11.1 wt % O, 7.8 wt % F and 1.1 wt % Al. The F and O elements are attributed to presence of –F, –OH, and –COOH.

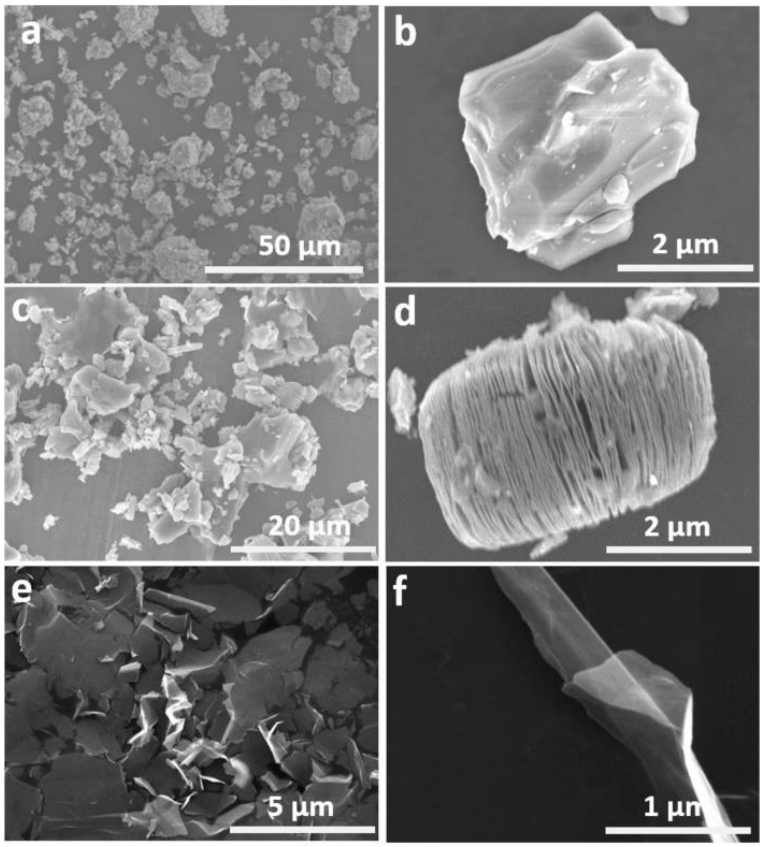

Figure 2. SEM images of Ti_3AlC_2 MAX (**a**) at a lower magnification, (**b**) at a higher magnification; SEM images of accordion-like multi-layered $Ti_3C_2T_x$ (**c**) at a lower magnification, (**d**) at a higher magnification); SEM images of $Ti_3C_2T_x$ nanosheets (**e**) at a lower magnification, and (**f**) at a higher magnification).

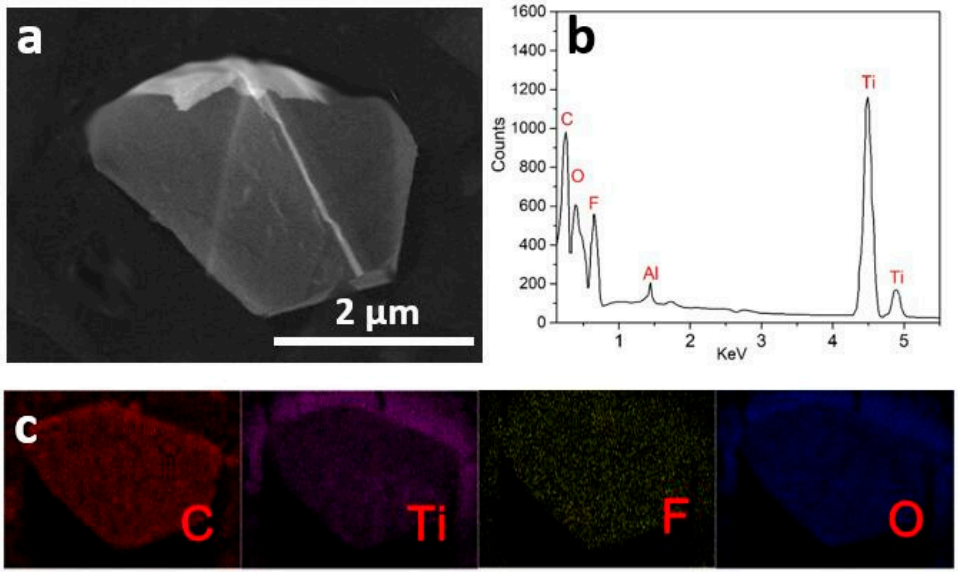

Figure 3. (**a**) SEM image of $Ti_3C_2T_x$ nanosheets, (**b**) energy-dispersive X-ray spectroscopy (EDX) spectrum of $Ti_3C_2T_x$ nanosheets, and (**c**) element mappings of $Ti_3C_2T_x$ nanosheets.

Table 1. Element content of $Ti_3C_2T_x$ MXene nanosheets.

Element	Atomic %	Weight %
C	27.4	11.0
Ti	40.8	69.0
O	19.0	11.1
F	11.6	7.8
Al	1.2	1.1

The structural properties of Ti_3AlC_2 and $Ti_3C_2T_x$ MXene were tested using XRD and Fourier transform infrared spectroscopy (FTIR), as shown in Figure 4. The diffraction pattern (Figure 4aA) has eleven broad peaks at 9.5°, 19.0°, 34.0°, 36.8°, 38.8°, 41.9°, 45.1°, 48.5°, 52.7°, 56.6°, and 60.2°, corresponding to (002), (004), (101), (103), (104), (105), (106), (107), (108), (109), and (110) of Ti_3AlC_2 MAX (JCPDS No. 52-0875) [28,29], respectively. It can be seen in the XRD patterns that the crystallinity and structural order of Ti_3AlC_2 decrease after HF treatment. As shown in Figure 4aB, no characteristic diffraction peaks of at 2θ = 36.9°, 38.9°, 42.0° belonged to Ti_3AlC_2 are observed (Figure 4aA) because of the removal of Al layers from Ti_3AlC_2 MAX. Moreover, the characteristic (002) peak at 2θ = 9.5° shifted to a lower value (2θ = 8.3°) and became broadened, displaying an increase in c-spacing when the Al atoms are removed away and replaced by –F and –OH. The FTIR spectra of Ti_3AlC_2 MAX and $Ti_3C_2T_x$ MXene nanosheets are shown in Figure 4b. There is no obvious peak in Ti_3AlC_2 MAX curve, which means there is no organic functional groups on Ti_3AlC_2 MAX. From Figure 4b, the obvious band at 3490 cm^{-1} is indicative of the presence of obvious strongly hydrogen-bonded –OH on the surface of $Ti_3C_2T_x$ MXene nanosheets. A weak peak at 1216 cm^{-1} can be observed. This weak peak is a characteristic of covalent C–F bond stretching vibrations [30]. FTIR result confirmed that Al atoms are replaced by –F, –OH, and –COOH functional groups, which is consistent with the XRD result.

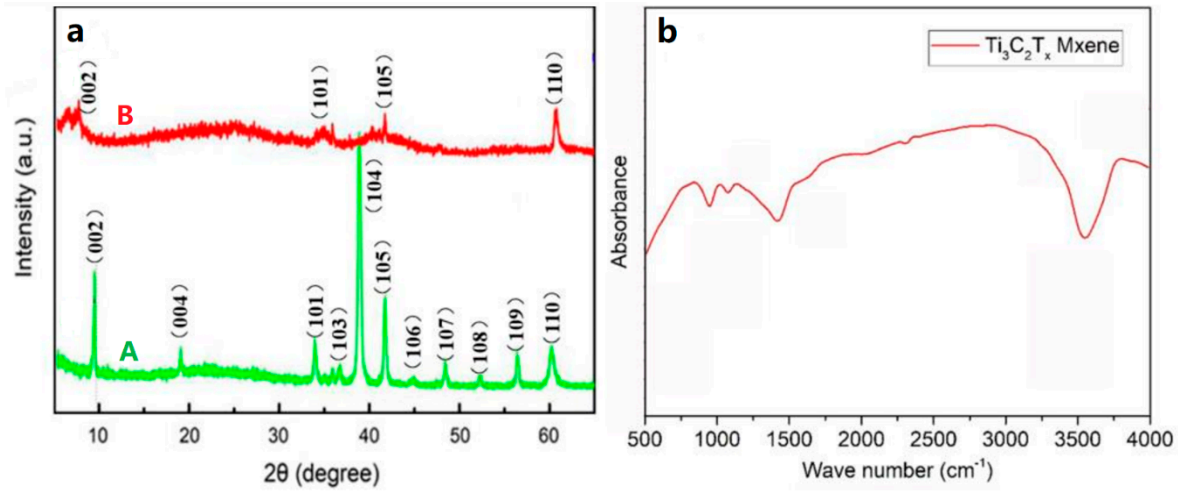

Figure 4. (**a**) XRD patterns of Ti_3AlC_2 MAX (A) and $Ti_3C_2T_x$ nanosheets (B). (**b**) FTIR spectra of $Ti_3C_2T_x$ nanosheets.

Figure 5 show TEM image and the corresponding selected-area electron diffraction (SAED) of $Ti_3C_2T_x$ MXene nanosheets. Figure 5a indicates a typical low-magnification TEM image of the synthesized $Ti_3C_2T_x$ MXene, in which thin nanosheet morphology formed, and the thin nanosheet has five layers, which is consistent with the SEM result. HRTEM was used to characterize the $Ti_3C_2T_x$ MXene nanosheets (Figure 5b). The $Ti_3C_2T_x$ MXene sample shows the characteristic spacings of 0.31 nm for the (110) lattice planes of $Ti_3C_2T_x$ [31]. The SAED pattern of $Ti_3C_2T_x$ MXene nanosheets showed a hexagonal arrangement at the atomic scale, revealing the typical hexagonal crystalline structure of $Ti_3C_2T_x$ phase.

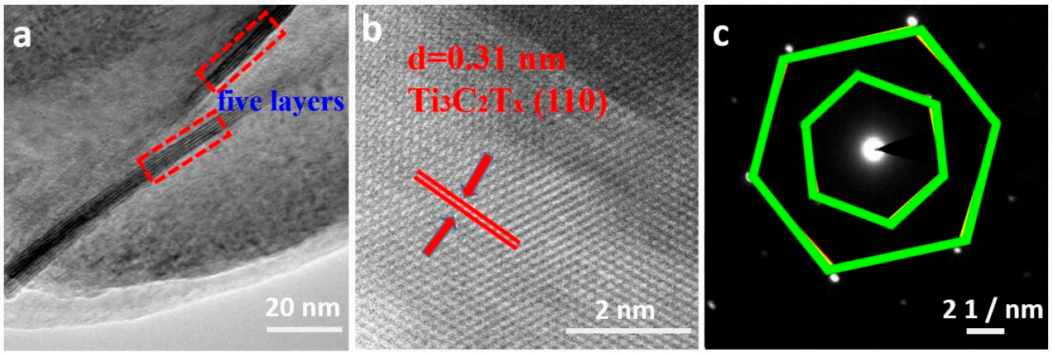

Figure 5. (**a**) TEM image of $Ti_3C_2T_x$ nanosheets, (**b**) HRTEM image of $Ti_3C_2T_x$ nanosheets, and (**c**) selected-area electron diffraction (SAED) of $Ti_3C_2T_x$ nanosheets.

3.2. The Structure of EP/$Ti_3C_2T_x$ MXene Nanosheets ECAs

Figure 6 shows XRD patterns of the epoxy (a), $Ti_3C_2T_x$ MXene nanosheets (b), EP/$Ti_3C_2T_x$ MXene nanosheets composite containing 0.4 wt % $Ti_3C_2T_x$ (c), EP/$Ti_3C_2T_x$ MXene nanosheets composite containing 1.0 wt % $Ti_3C_2T_x$ (d), and EP/$Ti_3C_2T_x$ MXene nanosheets composite containing 1.6 wt % $Ti_3C_2T_x$ (e). The epoxy has a broad peak at $2\theta = 16.8°$, whereas $Ti_3C_2T_x$ MXene nanosheets have peaks at $2\theta = 8.8°$, 60.2° belonged to (002) and (110) planes. For EP/$Ti_3C_2T_x$ MXene nanosheets composite, the characteristic (002) peak of $Ti_3C_2T_x$ MXene nanosheets shifted to a lower value. The EP composite containing 0.4 wt % filler did not give any discernible (002) or (110) peaks (Figure 6c), most likely because the $Ti_3C_2T_x$ loading was not sufficient to yield any signal. At a higher loading fraction of 1.0 wt %, the composite had the (110) peak and also a similar (002) peak shift. The EP composite containing 1.6 wt % still had the (110) peak which become broad. Explanation for this might be that EP polymer molecular chains are incorporated in the $Ti_3C_2T_x$ MXene layers which make the d-spacing increase.

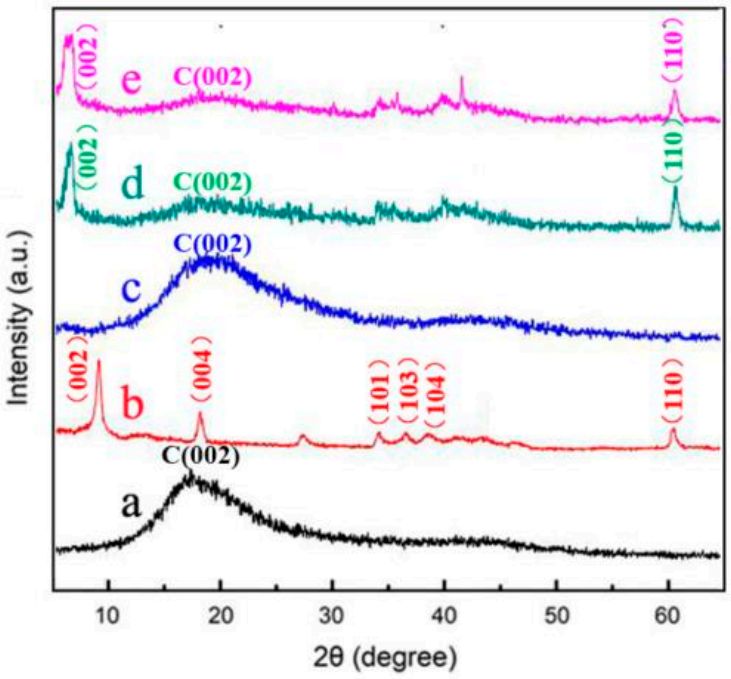

Figure 6. XRD patterns of epoxy (**a**), $Ti_3C_2T_x$ MXene nanosheets (**b**), EP/$Ti_3C_2T_x$ MXene nanosheets composite containing 0.4 wt % $Ti_3C_2T_x$ (**c**), EP/$Ti_3C_2T_x$ MXene nanosheets composite containing 1.0 wt % $Ti_3C_2T_x$ (**d**), and EP/$Ti_3C_2T_x$ MXene nanosheets composite containing 1.6 wt % $Ti_3C_2T_x$ (**e**).

3.3. Electrical Conductivity and Mechanical Performance

The electrical conductivity (K) of the EP/$Ti_3C_2T_x$ MXene nanosheets composite under various mass fractions of $Ti_3C_2T_x$ MXene nanosheets is illustrated in Figure 7. From Figure 7 we can observe that the electrical conductivity of the EP/$Ti_3C_2T_x$ MXene nanosheets composite increases gradually as the increasing of $Ti_3C_2T_x$ MXene nanosheets filler content. When the content of $Ti_3C_2T_x$ MXene nanosheets is lower than 0.4 wt %, the electrical conductivity slowly increases with increasing content of $Ti_3C_2T_x$ MXene nanosheets. When the content of $Ti_3C_2T_x$ MXene nanosheets increases to 0.6 wt %, the electrical conductivity of the EP/$Ti_3C_2T_x$ MXene nanosheets composite increases significantly. The critical content of filler is regarded as the percolation threshold. Thus the percolation threshold of the EP/$Ti_3C_2T_x$ MXene nanosheets composite is ~0.85 wt %. The electrical conductivity of the EP/$Ti_3C_2T_x$ MXene nanosheets composite in percolation threshold is 1.81×10^{-6} S/m, that is, ten orders of magnitude higher than that of the pure epoxy resin (about 1.03×10^{-16} S/m). After that, the electrical conductivity of the EP/$Ti_3C_2T_x$ MXene nanosheets composites also increases as the content of $Ti_3C_2T_x$ MXene nanosheets increases. However, its electrical conductivity increases slowly.

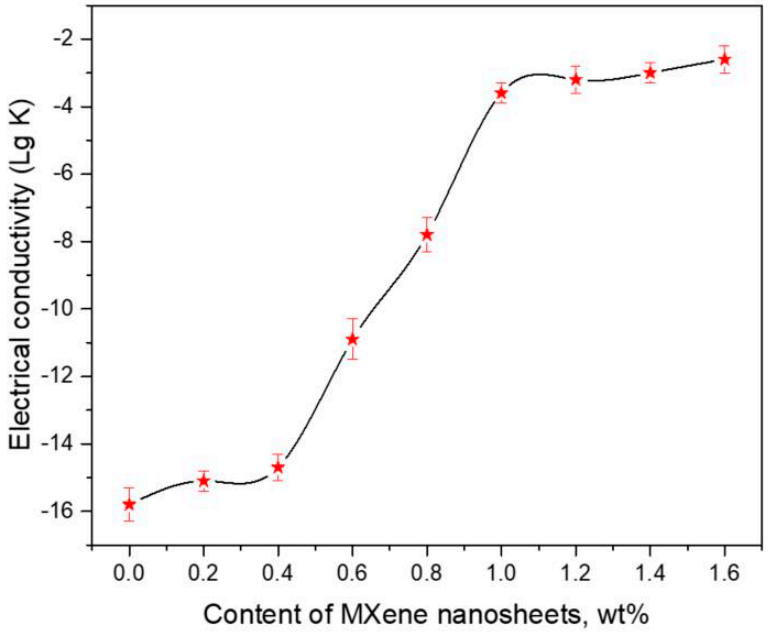

Figure 7. The electrical conductivity (K, S/m) of the EP/$Ti_3C_2T_x$ MXene nanosheets composite under various mass fractions of $Ti_3C_2T_x$ MXene nanosheets.

The percolation theory was applied for the calculation of the percolation threshold of composites. The dependence of the electrical conductivity of EP/$Ti_3C_2T_x$ MXene nanosheets composite on $Ti_3C_2T_x$ MXene content can be described in $\sigma_m = \sigma_n(P\text{-}Pc)^{\beta}$, where σ_n is the conductivity of $Ti_3C_2T_x$ MXene nanosheets, σ_m is the electrical conductivity of EP/$Ti_3C_2T_x$ MXene nanosheets composite, P is the volume fraction of $Ti_3C_2T_x$ MXene nanosheets, Pc is the percolation threshold, β is the conductivity exponent which is approximately 1.3 and 2.0 for three-dimensional and two-dimensions randomly distributed nanocomposites, respectively, in the percolation model [32]. The density of the $Ti_3C_2T_x$ MXene nanosheets is ~5 greater than the EP polymer. Therefore, we calculate that the conductivity exponent for EP/$Ti_3C_2T_x$ MXene nanosheets composite as $\beta = 0.84$. The $Ti_3C_2T_x$ MXene nanosheets electrical conductivity is about 24 S/cm which is much higher than conventional non-conductive polymer (~10^{-16} S/cm) and the $Ti_3C_2T_x$ MXene nanosheets have a large aspect ratio (~100–500), which can be observed in the SEM photograph of the $Ti_3C_2T_x$ MXene nanosheets. Such an extreme geometry might be a factor contributable to the high electrical conductivity and low conductivity exponent. We can infer that the percolation threshold of EP/$Ti_3C_2T_x$ MXene nanosheets composite is

about 0.28 vol % (0.85 wt %). The percolation threshold of EP/$Ti_3C_2T_x$ MXene nanosheets composite (0.85 wt %) is higher than that of aligned multi-wall carbon nanotube/EP composite (0.0025 wt %) because aligned CNT by an injection CVD method overcome the obstacle of aggregation and show higher electrical conductivity [32]. However, usually CNT is easy to aggregate in polymer composites, which hamper their high electrical conductivity. So the percolation threshold of our composite is lower than that of usual CNT-based polymer composite [33].

The mechanical properties (tensile strength and impact strength) of the EP/$Ti_3C_2T_x$ MXene nanosheets composite are tested with electronic tensile testing machine. The dependencies of tensile strength (a) and impact strength (b) of the EP/$Ti_3C_2T_x$ MXene nanosheets composite on the content of the $Ti_3C_2T_x$ MXene nanosheets are shown in Figure 8. Figure 8 shows that the tensile strength and impact strength of the EP/$Ti_3C_2T_x$ MXene nanosheets composite first increases with the content of $Ti_3C_2T_x$ MXene nanosheets increasing. When the content of $Ti_3C_2T_x$ MXene nanosheets increases to 1.2 wt %, the tensile strength and impact strength of composite arrive at the highest value of 66.2 MPa and 24.2 kJ/m^2, which is better than that in some papers [34]. After that, the tensile strength and impact strength of composite then gradually decreases. It is known that the tensile strength and impact strength of polymer resin is related to the rigidity of the polymer chains. As the content of $Ti_3C_2T_x$ MXene nanosheets increase, the rigidity of the EP/$Ti_3C_2T_x$ MXene nanosheets composite increases due to $Ti_3C_2T_x$ MXene nanosheets that connect many single EP polymer chains by –F, –OH, and –COOH functional groups. However, when the content of $Ti_3C_2T_x$ MXene nanosheets is more than 1.2 wt %, the EP/$Ti_3C_2T_x$ MXene nanosheets composite possesses more $Ti_3C_2T_x$ MXene nanosheets agglomeration, reducing their tensile strength and impact strength.

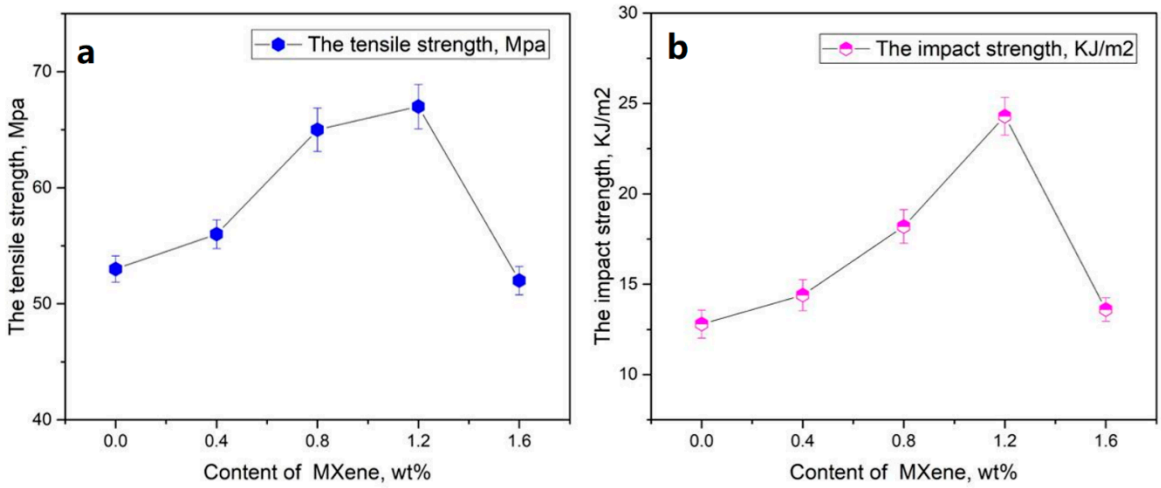

Figure 8. The (**a**) tensile strength and (**b**) impact strength of the EP/$Ti_3C_2T_x$ MXene nanosheets composite under various contents of the $Ti_3C_2T_x$ MXene nanosheets.

3.4. The Morphology of EP/$Ti_3C_2T_x$ MXene Nanosheets Composite

To understand the effect of the content of $Ti_3C_2T_x$ Mxene nanosheets in NH_2–CF/MXene/EP composites on mechanical properties, SEM was used to observe the fracture surfaces of EP composites after impact strength test. Figure 9a–d presents the fracture source of EP/$Ti_3C_2T_x$ MXene nanosheets composite containing 0.4 wt %, 0.8 wt %, 1.2 wt %, and 1.6 wt % $Ti_3C_2T_x$ MXene nanosheets. The EP/$Ti_3C_2T_x$ MXene nanosheets composite containing 0.4 wt % $Ti_3C_2T_x$ MXene nanosheets display comparatively slippery fracture (Figure 9a). The fracture surfaces of EP/$Ti_3C_2T_x$ MXene nanosheets composite containing 0.8 wt % or 1.2 wt % $Ti_3C_2T_x$ MXene nanosheets are rougher. In Figure 9d, we can observe that there is apparent agglomeration on the fracture surface of EP/$Ti_3C_2T_x$ MXene nanosheets composite containing 1.6 wt % $Ti_3C_2T_x$ MXene nanosheets. The agglomeration of $Ti_3C_2T_x$

MXene nanosheets could decrease the impact strength of the EP composites. So the SEM results are consistent with the impact strength shown in Figure 8b.

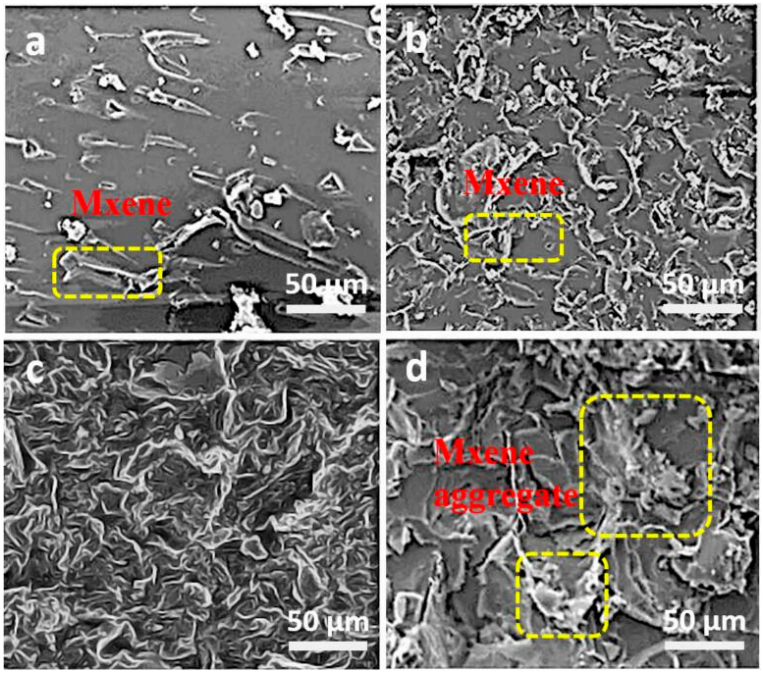

Figure 9. The fracture surfaces of the EP/$Ti_3C_2T_x$ MXene nanosheets composite containing 0.4 wt % $Ti_3C_2T_x$ MXene nanosheets (**a**), 0.8 wt % $Ti_3C_2T_x$ MXene nanosheets (**b**), 1.2 wt % $Ti_3C_2T_x$ MXene nanosheets (**c**), and 1.6 wt % $Ti_3C_2T_x$ MXene nanosheets (**d**).

4. Conclusions

In summary, a novel ECA based on EP resin filled with $Ti_3C_2T_x$ MXene nanosheets was prepared by a simple solution blending. $Ti_3C_2T_x$ MXene is of nanosheet structure, which contains 11.0 wt % C, 69.0 wt % Ti, 11.1 wt % O, 7.8 wt % F, and 1.1 wt % Al. These –F, –OH, and –COOH functional groups make $Ti_3C_2T_x$ MXene nanosheets homogeneously disperse in EP resin. The electrical conductivity of the EP/$Ti_3C_2T_x$ MXene nanosheets composite increases gradually as $Ti_3C_2T_x$ MXene nanosheets content increases, and the percolation threshold of EP/$Ti_3C_2T_x$ MXene nanosheets composite is 0.85 wt %. The electrical conductivity of EP/$Ti_3C_2T_x$ MXene nanosheets composite in percolation threshold is 1.81×10^{-6} S/m, which is ten orders of magnitude higher than that of the pure epoxy resin (~1.03×10^{-16} S/m). The increase in $Ti_3C_2T_x$ MXene nanosheets content may increase the tensile strength and impact strength of epoxy/$Ti_3C_2T_x$ MXene nanosheets composite when the content of filler is low. When the content of filler is 1.2 wt %, the properties of epoxy/$Ti_3C_2T_x$ MXene nanosheets composite are optimum (electrical conductivity of 4.52×10^{-4} S/m, tensile strength of 66.2 MPa and impact strength of 24.2 KJ/m^2). This work presents more applications of MXene-polymer composites.

Author Contributions: A.F. conceived the idea of the paper; T.H. collected and classified the related literature; Z.J. and G.W. also gave helpful advice during the writing process. Y.Z. and F.Z. also gave some great enlightenment and helpful advices during calculating the percolation threshold and the revising process. A.F. wrote the paper. All authors have read and agreed to the published version of the manuscript.

Funding: This work was financially supported by the Natural Science Foundation of Shandong Province (No. ZR2019YQ24), the Qingchuang Talents Induction Program of Shandong Higher Education Institution (Research and Innovation Team of Structural–Functional Polymer Composites), National Natural Science Foundation of China (No. 51407134, No. 51801001), China Postdoctoral Science Foundation (No. 2016M590619, No. 2016M601878), Qingdao Postdoctoral Application Research Project, Provincial Key Research and Development Program of Shaanxi (No. 2019GY-197), Key Laboratory of Engineering Dielectrics and Its Application (Harbin University of Science and Technology), Ministry of Education (No. KFZ1803), Key Project of Baoji University of Arts and Sciences (No. ZK2018051), Baoji Science and Technology Project (No. 16RKX1-29) and Baoji Engineering Technology

Research Center for Ultrafast Optics and New Materials (No. 2015CXNL-1-3). Feng AL is supported by The Thousand Talents Plan for Young Professionals of Shaanxi Province.

Acknowledgments: The authors thank the colleagues in the laboratory for their support.

Conflicts of Interest: The authors declare no conflicts of interest.

References

1. Jakubinek, M.B.; Ashrafi, B.; Zhang, Y.; Martinez-Rubi, Y.; Kingston, C.T.; Johnston, A.; Simard, B. Single-walled carbon nanotube—Epoxy composites for structural and conductive aerospace adhesives. *Compos. Part B* **2015**, *69*, 87–93. [CrossRef]
2. Hou, T.; Wang, B.; Jia, Z.; Wu, H.; Lan, D.; Huang, Z.; Feng, A.; Ma, M.; Wu, G. A review of metal oxide-related microwave absorbing materials from the dimension and morphology perspective. *J. Mater. Sci.* **2019**, *30*, 10961–10984. [CrossRef]
3. Rubinstein, M.; Colby, R.H. *Polymer Physics*; Oxford university press: New York, NY, USA, 2003; pp. 88–89.
4. Feng, A.; Wu, G.; Pan, C.; Wang, Y. Synthesis, preparation and mechanical property of wood fiber-reinforced poly (vinyl chloride) composites. *J. Nanosci. Nanotechnol.* **2017**, *17*, 3859–3863. [CrossRef]
5. Tyson, W.R.; Miller, W.A. Surface free energies of solid metals: Estimation from liquid surface tension measurements. *Surf. Sci.* **1977**, *62*, 267–276. [CrossRef]
6. Wu, G.L.; Cheng, Y.H.; Yang, Z.H.; Jia, Z.R.; Wu, H.J.; Yang, L.J.; Li, H.L.; Guo, P.Z.; Lv, H.L. Design of Carbon Sphere/Magnetic Quantum Dots with Tunable Phase Compositions and Boost Dielectric Loss Behavior. *Chem. Eng. J.* **2018**, *333*, 519–528. [CrossRef]
7. Kurlyandskaya, G.V.; Safronov, A.P.; Terzian, T.V.; Volodina, N.S.; Beketov, I.V.; Lezama, L.; Prieto, L.M. $Fe_{45}Ni_{55}$ magnetic nanoparticles obtained by electric explosion of wire for the development of functional composites. *IEEE Magn. Lett.* **2015**, *6*, 1–4. [CrossRef]
8. Zhou, X.F.; Jia, Z.R.; Feng, A.L.; Wang, X.X.; Liu, J.J.; Zhang, M.; Cao, H.J.; Wu, G.L. Synthesis of fish skin -derived 3D carbon foams with broadened bandwidth and excellent electromagnetic wave absorption performance. *Carbon* **2019**, *152*, 827–836. [CrossRef]
9. Gao, Z.G.; Xu, B.H.; Ma, M.L.; Feng, A.L.; Zhang, Y.; Liu, X.H.; Jia, Z.R.; Wu, G.L. Electrostatic self-assembly synthesis of $ZnFe_2O_4$ quantum dots ($ZnFe_2O_4$@C) and electromagnetic microwave absorption. *Compos. Part B* **2019**, *179*, 107417. [CrossRef]
10. Li, Z.; Le, T.; Wu, Z.; Yao, Y.; Li, L.; Tentzeris, M.; Moon, K.; Wong, C.P. Rational Design of a Printable, Highly Conductive Silicone-based Electrically Conductive Adhesive for Stretchable Radio-Frequency Antennas. *Adv. Funct. Mater.* **2015**, *25*, 464–470. [CrossRef]
11. Du, Z.X.; Li, J.X. The synthesis, structure and magnetic properties of a mononuclear cobalt compound with dipyrimidine sulfane ligand derived from 2-thio-barbituric acid. *Inorg. Chim. Acta* **2015**, *436*, 159–162. [CrossRef]
12. Li, J.X.; Du, Z.X.; Wang, J.G.; Wang, T.; Lv, J.N. Zinc and manganese coordination polymers constructed by a new coordination mode of 4,5-dicyanoimidazolate ligand: Syntheses, crystal structures, fluorescent and magnetic properties. *Inorg. Chem. Commun.* **2012**, *15*, 243–247. [CrossRef]
13. Ren, H.; Guo, Y.; Huang, S.; Zhang, K.; Yuen, M.; Fu, X.; Yu, S.; Sun, R.; Wong, C. One-step preparation of silver hexagonal microsheets as electrically conductive adhesive fillers for printed electronics. *ACS Appl. Mater. Int.* **2015**, *7*, 13685–13692. [CrossRef] [PubMed]
14. Wu, G.L.; Jia, Z.R.; Zhou, X.F.; Nie, G.Z.; Lv, H.L. Interlayer Controllable of Hierarchical MWCNTs@C@Fe_xO_y Cross-linked Composite with Wideband Electromagnetic Absorption Performance. *Compos. Part A* **2020**, *128*, 105687. [CrossRef]
15. Wu, W.; Yu, C.; Chen, J.; Yang, Q. Fluorometric detection of copper ions using click chemistry and the target-induced conjunction of split DNAzyme fragments. *Int. J. Environ. Anal. Chem.* **2019**. [CrossRef]
16. Jia, Z.R.; Wang, C.; Feng, A.L.; Shi, P.B.; Zhang, C.H.; Liu, X.H.; Wang, K.K.; Wu, G.L. A low dielectric decoration strategy to achieve absorption dominated electromagnetic shielding material. *Compos. Part B* **2020**, *183*, 107690. [CrossRef]
17. Pan, C.; Zhang, J.Q.; Kou, K.C.; Zhang, Y.; Wu, G.L. Investigation of the through-plane thermal conductivity of polymer composites with in-plane oriented hexagonal boron nitride. *Int. J. Heat Mass Tran.* **2018**, *120*, 1–8. [CrossRef]

18. Jia, Z.R.; Wang, B.B.; Feng, A.L.; Liu, J.J.; Zhang, C.H.; Zhang, M.; Wu, G.L. Fabrication of $Ni_xCo_{3-x}S_4$ hollow nanosphere as wideband electromagnetic absorber at thin matched thickness. *Ceram. Int.* **2019**, *45*, 15854–15859. [CrossRef]
19. Zhao, J.; Zhang, D. Epoxy-based adhesives filled with flakes Ag-coated copper as conductive fillers. *Polym. Compos.* **2017**, *38*, 846–851. [CrossRef]
20. Li, J.X.; Du, Z.X.; Feng, X. A new binuclear Ni^{II} complex with tetrafluorophthalate and 2,2′-bipyridine ligands: Synthesis, crystal structure and magnetic properties. *Z. Naturforsch.* **2019**, *74*, 833–838. [CrossRef]
21. Li, J.X.; Du, Z.X.; Wang, J.; Feng, X. Two mononuclear zinc(II) complexes constructed by two types of phenoxyacetic acid ligands: Syntheses, crystal structures and fluorescence properties. *Z. Naturforsch.* **2019**, *74*, 839–845. [CrossRef]
22. Li, J.X.; Du, Z.X.; Bai, R.F. Crystal structure of aqua-bis(5-bromo-6-methyl-picolinato-κ^2N,O)zinc(II) dihydrate, $C_{14}H_{16}Br_2N_2O_7Zn$. *Z. Krist. New Cryst. Struct.* **2019**, *235*, 63–65. [CrossRef]
23. Li, J.X.; Du, Z.X. A Binuclear Cadmium (II) Cluster Based on π–π Stacking and Halogen-Halogen Interactions: Synthesis, Crystal Analysis and Fluorescent Properties. *J. Clust. Sci.* **2019**, *22*, 1–5. [CrossRef]
24. Feng, A.; Ma, M.; Jia, Z.; Zhang, M.; Wu, G. Fabrication of $NiFe_2O_4$@carbon fiber coated with phytic acid-doped polyaniline composite and its application as an electromagnetic wave absorber. *RSC Adv.* **2019**, *9*, 25932–25941. [CrossRef]
25. Simon, P. Two-dimensional MXene with controlled interlayer spacing for electrochemical energy storage. *ACS Nano* **2017**, *11*, 2393. [CrossRef]
26. Ding, L.; Wei, Y.; Li, L.; Zhang, T.; Wang, H.; Xue, J.; Ding, L.; Wang, S.; Caro, J.; Gogotsi, Y. MXene molecular sieving membranes for highly efficient gas separation. *Nat. Commun.* **2018**, *9*, 155. [CrossRef]
27. Nam, S.; Umrao, S.; Oh, S.; Shin, K.H.; Park, H.S.; Oh, I.K. Sonochemical self-growth of functionalized titanium carbide nanorods on Ti_3C_2 nanosheets for high capacity anode for lithium-ion batteries. *Compos. Part B* **2020**, *181*, 107583. [CrossRef]
28. Ahmed, B.; Anjum, D.H.; Gogotsi, Y.; Alshareef, H. Atomic layer deposition of SnO_2 on MXene for Li-ion battery anodes. *Nano Energy* **2017**, *34*, 249–256. [CrossRef]
29. Hou, T.; Wang, B.B.; Ma, M.L.; Feng, A.L.; Huang, Z.Y.; Zhang, Y.; Jia, Z.; Tan, G.X.; Cao, H.J.; Wu, G.L. Preparation of two-dimensional titanium carbide ($Ti_3C_2T_x$ and $NiCo_2O_4$ composites to achieve excellent microwave absorption properties. *Compos. Part B* **2020**, *180*, 107577. [CrossRef]
30. Wang, F.; Cao, M.; Qin, Y.; Zhu, J.; Wang, L.; Tang, Y. ZnO nanoparticle-decorated two-dimensional titanium carbide with enhanced supercapacitive performance. *RSC Adv.* **2016**, *6*, 88934–88942. [CrossRef]
31. Zhang, Y.; Guo, B.; Hu, L.; Xu, Q.; Li, Y.; Liu, D.; Xu, M. Synthesis of SnS nanoparticle-modified MXene ($Ti_3C_2T_x$) composites for enhanced sodium storage. *J. Alloys Compd.* **2018**, *732*, 448–453. [CrossRef]
32. Sandler, J.; Kirk, J.E.; Kinloch, I.A.; Shaffer, M.S.P.; Windle, A.H. Ultra-low electrical percolation threshold in carbon-nanotube-epoxy composites. *Polymer* **2003**, *44*, 5893–5899. [CrossRef]
33. Tjong, S.C.; Liang, G.D.; Bao, S.P. Electrical behavior of polypropylene/multiwalled carbon nanotube nanocomposites with low percolation threshold. *Scr. Mater.* **2007**, *57*, 461–464. [CrossRef]
34. Lu, T.; Jiang, M.; Jiang, Z.; Hui, D.; Wang, Z.; Zhou, Z. Effect of surface modification of bamboo cellulose fibers on mechanical properties of cellulose/epoxy composites. *Compos. Part B* **2013**, *51*, 28–34. [CrossRef]